Dispersions and attenuations in a fully saturated sandstone: Experimental evidence for fluid flows at different scales

Lucas Pimienta[1], Jérôme Fortin[1], Jan V. M. Borgomano[1], and Yves Guéguen[1]

Abstract

Dispersion and attenuation of elastic waves have been observed in crustal rocks. Existing theories and experimental measurements evidenced the existence of different energy-loss mechanisms. In rocks fully saturated by a Newtonian fluid, one major candidate is fluid flow at different scales, separating three regimes: the drained, undrained, and unrelaxed regimes. Here, two elastic transitions, between these three regimes, are investigated. Both the cause and the consequence of the drained/undrained transition are evidenced. Because the second transition measured occurs at higher frequency, where no global fluid flow occurs, it in turn is associated to the undrained/unrelaxed transition (or squirt flow). For both transitions, the amount of open microcracks seems to be the major contributor to the magnitudes of attenuation.

Introduction

Frequency dependence of "elastic" properties is a well-known characteristic of viscoelastic materials. Is it the case for fluid-saturated rocks? In such materials, various loss mechanisms have been identified, such as (Batzle et al., 2014) squirt flow in fully saturated rocks, pocket flow in partially saturated rocks, or even intrinsic loss in the fluid phase alone. Experimental methods were devised to better characterize those effects, one of which is the stress-strain (or forced-deformation) method. Starting from Spencer Jr. (1981), and with the pioneering work of Batzle et al. (2001, 2005, 2006), this latter method has shown promise. Recently, more teams have developed apparatuses using this method to increase the current knowledge on those frequency effects.

Here, we are interested in the dispersion and attenuation effects occurring in fully saturated sedimentary rocks, which are thought to originate from fluid flow at different scales. A new protocol is designed to jointly investigate two elastic dispersion and attenuation phenomena. Moreover, using two distinct setups, the frequency dependence of a rock's bulk modulus, Young's modulus, and Poisson's ratio are reported.

Note that each existing experimental setup has its intrinsic characteristics that need to be properly assessed in order to compare and generalize the measured properties. This last aspect is investigated using a simple analytical poroelastic model.

Measuring frequency effects in fully saturated rocks

Elastic regimes in rocks: Evidence for transitions between regimes? In fully saturated sedimentary rocks, as detailed by Hofmann (2006), several dispersion/attenuation phenomena may occur. Here, we are interested in three main elastic regimes that have been shown to exist: the drained, undrained, and unrelaxed regimes.

The drained regime is that in which fluid is allowed to flow in and out of a representative elementary volume (REV). Because fluid is free to flow out, it does not pressurize inside the REV so that the drained regime is theoretically independent of the saturating fluid. In the undrained regime, fluid is not allowed to flow out of the REV and pressurizes in response to the applied pressure. For a given applied pressure, the volumetric strain is larger under drained conditions than in undrained ones. As a consequence, the rock's bulk modulus is stiffer in undrained conditions, i.e., $K_{ud} > K_d$. Experimentally, drained (Figure 1a) and undrained (Figure 1b) regimes usually can be measured by changing the boundary conditions at the sample scale.

The third regime is that in which fluid has no time to flow locally from one inclusion to the next one. In this final case, the fluid is not isobaric at the scale of the REV anymore. The regime is called "unrelaxed" (Figure 1c). It can be found intuitively that (1) the buildup pore fluid pressure inside the different inclusions intrinsically depends on the inclusion's geometry; and (2) the buildup pressure in the compressible defects is much higher than it is in the undrained regime. The resulting compressibility of the medium decreases, leading to the relations: $K_{ur} > K_{ud}$ and $G_{ur} > G_{ud}$. At this stage, fluid is expected to contribute to the rock's response to a shear solicitation, leading to the increase in the shear modulus.

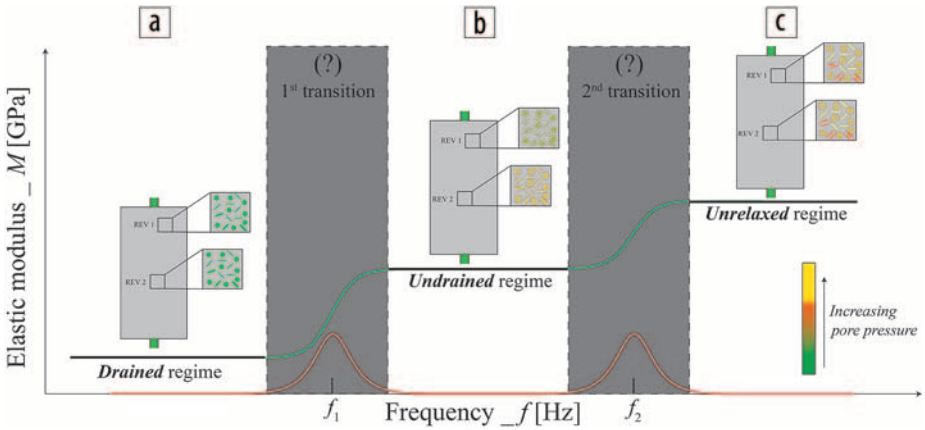

Figure 1. Schematics of the (a) drained, (b) undrained, and (c) unrelaxed regimes plotted as a function of expected frequency dependence and values of elastic moduli. The three regimes are known theoretically. The question remains for the transition between those regimes, in terms of dispersion (i.e., green curves) and attenuation (i.e., red curves) phenomena.

[1]PSL Research University, Laboratoire de Géologie de l'ENS.

http://dx.doi.org/10.1190/tle35060495.1.

Experimentally, drained (Figure 1a) and unrelaxed (Figure 1c) regimes can be obtained respectively from the measured ultrasonic wave velocities under dry and liquid-saturated conditions.

While, theoretically, it is expected to observe three regimes in the seismic frequency range (O'Connell and Budiansky, 1977; Cleary, 1978), the evolution of the elastic properties between these regimes is poorly known (Figure 1). Although several models intended to predict these elastic transitions (e.g., Müller et al., 2010), no direct measurements allowed confirmation of these models.

In case of a viscoelastic-like response, a frequency-dependent increase in elastic properties should relate with a dissipation peak. Should one expect similar behaviors for the transitions between those elastic regimes?

Experimental setup and approach for the measurements. In addition to the ultrasonic wave velocity measurements, two setups have been used in this study to measure the frequency dependence of elastic moduli: the hydrostatic (Figure 2a) and axial (Figure 2b) setups. Each setup bears its intrinsic shortcomings that need to be fully understood and calibrated prior to applying the methodology to fluid-saturated rocks.

For both methods, calibrations were carried out using three standard homogeneous samples chosen for their range in elastic properties and because they do not depend on confining pressure. The samples are (1) an amorphous elastic glass sample; (2) a gypsum sample, also elastic in the pressure/temperature conditions of the experiment; and (3) a viscoelastic plexiglass sample. Consistent values and behaviors of their bulk modulus, Young's modulus, and Poisson's ratio are measured in the pressure and frequency domains of study. The frequency range attained by the experimental setups is (1) $f \in [10^{-3}; 10^{0}]$ Hz for the isotropic solicitation (Figure 2a); and (2) $f \in [10^{-3}; 10^{2}]$ Hz for the axial solicitation (Figure 2b). More details can be found on the calibrations, and measuring procedure, in Pimienta et al. (2015a, 2015b, 2016a).

For this study, a Fontainebleau sandstone sample of 7% porosity and 2 10^{-15} m^2 permeability is used to investigate those frequency effects. This rock was chosen because it is a clean sandstone (i.e., 100% quartz), homogeneous and isotropic at the sample scale, with well-characterized elastic and transport properties. The elastic properties of the sample, saturated by different fluids, are measured as a function of pressure and frequency. Experimental results on a 19% porosity Berea sandstone are also briefly introduced. This second rock has a high (about 90%) quartz content and essentially differs from Fo7 due to its higher porosity. The fluid's viscosity being a ruling parameter for the characteristic frequency of the phenomena (e.g., Batzle et al., 2006), viscous glycerine is used as a complement to water and air. An "apparent frequency" parameter $f^* = f(\eta/\eta_0)$ is defined, where η_0 and η are, respectively, the viscosity of water and of the fluid used, which allows us to account for the fluid viscosity in the same way as the frequency f. For a frequency range allowed of $f \in [10^{-3}; 10^{0}]$ Hz (i.e. isotropic solicitation), the range in apparent frequency reached is of $f^* \in [10^{-3}; 10^{3}]$ Hz.

Drained to undrained transition: Global flow

The first transition has been investigated here using a new methodology (Pimienta et al., 2015a). A large dead volume has been maintained at both ends of the sample, and fluid pressure (p_f) is measured in this dead volume to gain further insights on the mechanism at hand. From this methodology, four properties can be obtained using the strain and pore-pressure amplitudes and phases. The strain amplitude and phase lead to measurement of bulk modulus and associated dissipation, i.e., the sample *elastic response*. The pore-pressure amplitude and phase lead to measuring a so-called "pseudo-Skempton coefficient" (Pimienta et al., 2015a) and the pore fluid phase shift, i.e., the sample *hydraulic response*.

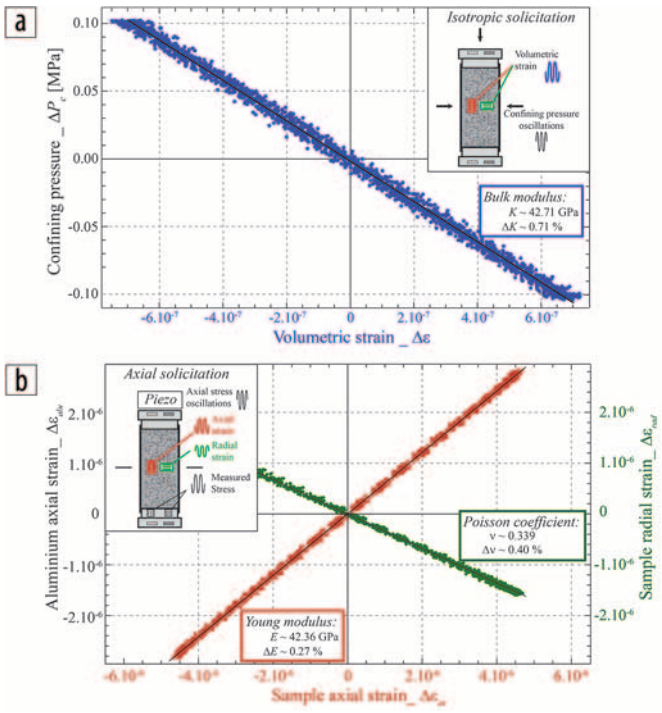

Figure 2. Schematics of the two solicitation modes calibrated and used in this study, associated to the corresponding linear regression for the case of the gypsum sample. (a) The isotropic solicitation mode relies on confining pressure oscillations and allows for measuring the bulk modulus and its dissipation as a function of frequency. (b) The axial solicitation relates to oscillations of axial stress and allows for measuring Young's modulus and Poisson's ratio, and their dissipations, as a function of frequency.

Under quasistatic conditions, the "pseudo-Skempton coefficient" would be the experimentally measured Skempton coefficient. However, the measurement here is dynamic (i.e., as a function of frequency) and characterizes the amount of fluid flow out of the sample during the oscillation. Indeed, because the dead volume is mechanically unaffected by the confining pressure oscillations, the measured fluid overpressures relate to a fluid mass/volume transferred from the sample to the dead volume where it pressurizes. The total fluid volume (V_f) is composed of the dead volume (V_d) and the sample pore volume (V_p) such that $V_f = (V_d + V_p)$. Because V_d is assumed to be independent of pressure, one gets $\Delta V_p = \Delta V_f = (V_t/K_f)\, p_f$, where K_f is the fluid bulk modulus.

The sample elastic and hydraulic response can then be obtained as a function of f^*. For the 7% porosity Fontainebleau sandstone sample, measured at a Terzaghi effective pressure of 1 MPa, a clear dispersion/attenuation is observed from the elastic response (Figures 3a and 3b). This dispersion/attenuation phenomenon

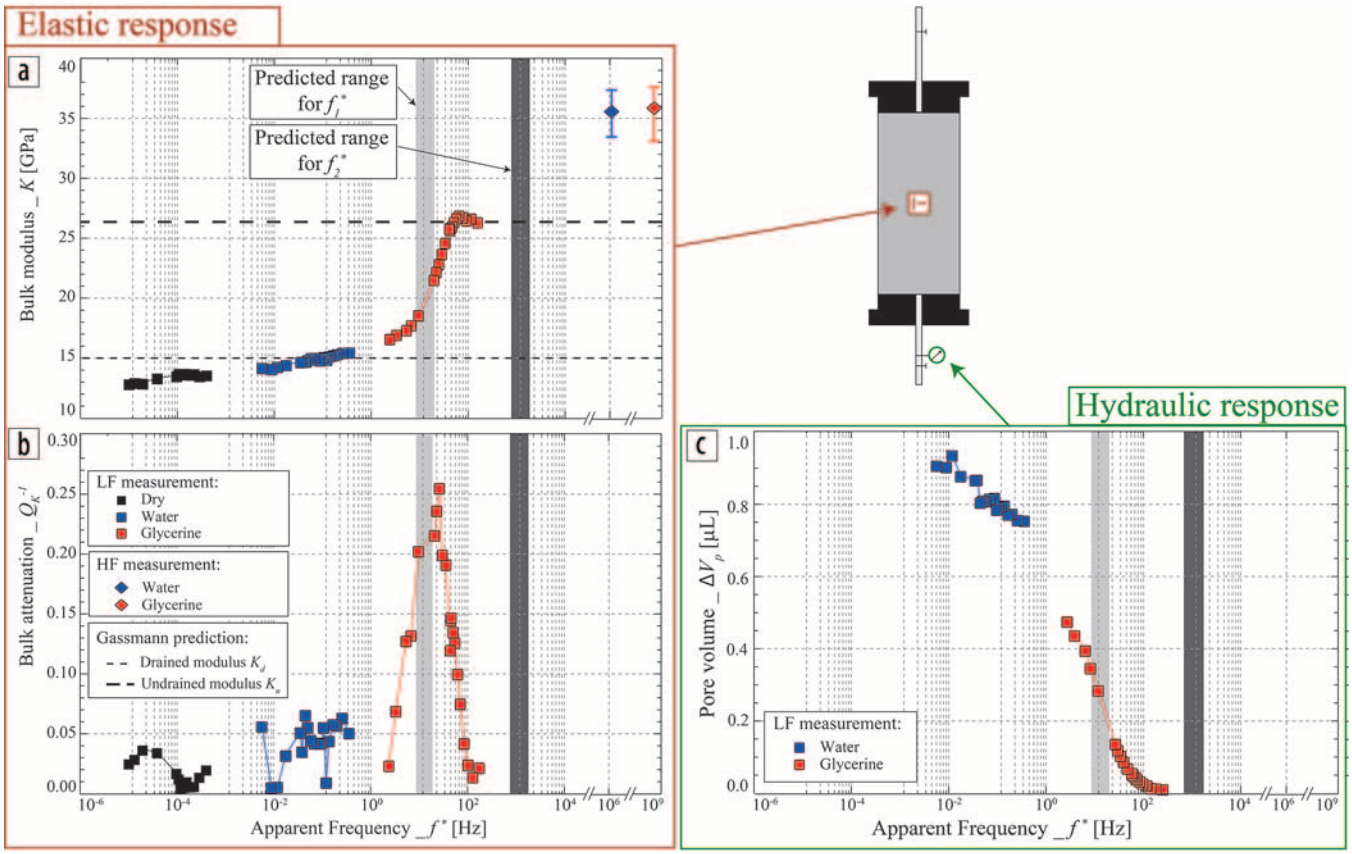

Figure 3. Example of the properties measured as a function of f^* on the 7% porosity Fontainebleau sample at an effective pressure of 1 MPa. The (a) bulk modulus and (b) its associated dissipation represent the elastic response. The (c) pore fluid volume ejected out of the sample represents the hydraulic response. Figure modified from Pimienta et al. (2015a).

has a form very similar to that of a standard viscoelastic material. The question is: What could be the cause of such dispersion/attenuation phenomenon?

The answer lies in the measured hydraulic response (Figure 3c). Transforming the measured pore fluid pressure (i.e., pseudo-Skempton parameter) in a pore volume (ΔV_f) ejected out of the sample, a clear transition is observed between fluid flow at low f^* to no fluid flow at higher f^*.

The dispersion/attenuation phenomenon measured fully correlates to the frequency-dependent disappearance of fluid flow out of the sample. Those measurements, thus, directly highlight both the cause (i.e., global fluid flow) and the consequence (i.e., dispersion/attenuation) of the transition from drained to undrained elastic regimes. Both fluid-flow (O'Connell and Budiansky, 1977; Cleary, 1978) and Biot-Gassmann theories show a consistent fit with the measurement (Figure 3a).

Undrained/unrelaxed transition: Squirt flow

While the system for "isotropic solicitation" allowed for investigating a range in frequencies of $f^* \in [10^{-3}; 10^{3}]$ Hz, the "axial solicitation" allows to go as high as $f^* \in [10^{-3}; 10^{5}]$ Hz. For the sample of interest, this allows both to measure the drained/undrained transition under water saturation (Figure 3) and to go beyond the drained/undrained transition under glycerine saturation. With this additional setup, Young's modulus and Poisson's ratio are the properties measured as a function of frequency.

The dependence of Young's modulus to the apparent frequency f^* is reported for an effective pressure of 1 MPa (Figure 4). Strong frequency-dependent variations in elastic properties are measured at all frequencies. Comparing, for example, the measured K (Figure 4a) and E values (Figure 4b) for this rock sample shows that the axial solicitation setup introduces further frequency-dependent increase, up to the ultrasonic value measured.

Using again the hydraulic properties of the sample, now in terms of a pseudoconsolidation parameter (Pimienta et al., 2015b), evidence for the disappearance of global fluid flow is observed at about f^* = 100 Hz. Consistent with the isotropic solicitation (Figure 3c), the sample is thus undrained at this value of f^*. Further dispersion/attenuation beyond it indicates a second physical transition measured on Young's modulus (Figure 4b).

Comparing the measurement to the theoretical cutoff frequencies, an overall consistency is observed. The first cutoff frequency (at f_1^* = 10 Hz) for the drained/undrained transition corresponds to the first dispersion/attenuation measured. The second cutoff frequency (at f_2^* = 1 kHz) for the undrained/unrelaxed transition fits with the second dispersion/attenuation measured. This indicates that the second dispersion/attenuation probably relates to the squirt-flow phenomenon responsible for the transition from the undrained to the unrelaxed regime.

One can use the Zener viscoelastic model to approximately compare the frequency-dependent variations of both groups of data on K (Figure 4a) and E (Figure 4b). The first (drained/

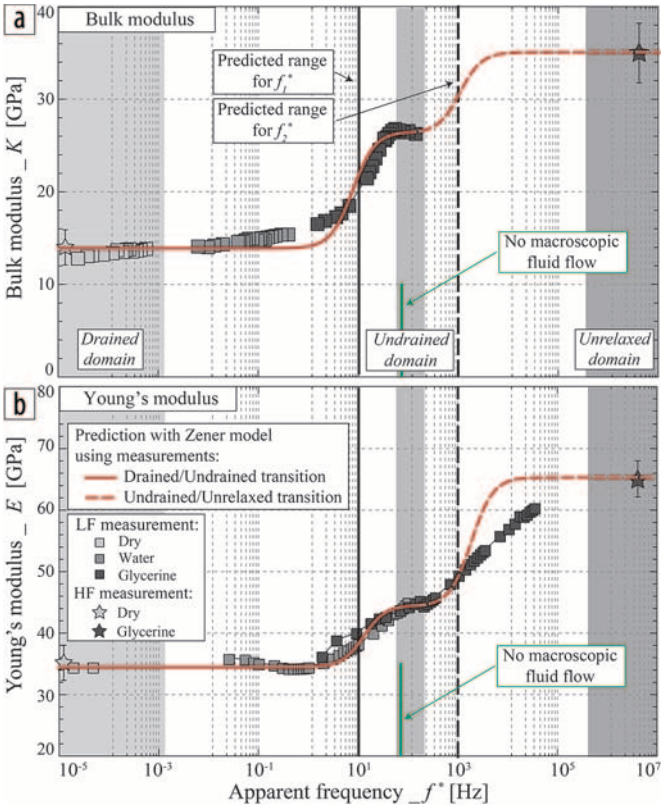

Figure 4. Comparison of the measured (a) bulk modulus (isotropic solicitation) and (b) Young's modulus (axial solicitation) for the 7% porosity sample at an effective pressure of 1 MPa. The expected zones for the three different regimes are highlighted as grayish zones, and the theoretical cutoff frequencies are reported. The measurements are compared with the expected frequency dependence for a typical viscoelastic Zener model. The experimental evidence for no macroscopic fluid flow is highlighted in green. Figure modified from Pimienta et al. (2015b).

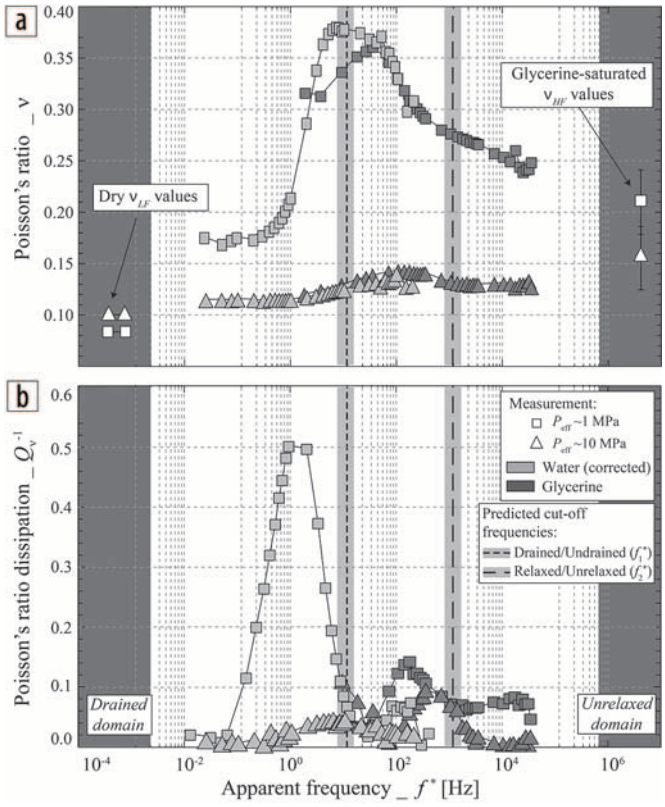

Figure 5. Measured (a) Poisson's ratio and (b) its dissipation as a function of apparent frequency for the 7% porosity Fontainebleau sandstone at two effective pressures of 1 MPa and 10 MPa. The two theoretical cutoff frequencies, for the drained/undrained and undrained/unrelaxed transitions respectively, are reported for comparison. The data at 1 MPa have been corrected using a poroelastic correction. Figure from Pimienta et al. (2016a).

undrained) fits the Zener model well. The second (undrained/unrelaxed) is spread over a large frequency range. This implies that there is a single relaxation time for the drained/undrained transition. This is not the case for the undrained/unrelaxed transition. Because the dominant parameter for the undrained/unrelaxed transition is the microcracks aspect ratio (O'Connell and Budiansky, 1977), this measurement may indicate the existence of a family of microcracks with varying aspect ratio inside the rock sample.

Implications for Poisson's ratio over the frequency range

From the radial and axial strain-gauges data, it is also possible to attain Poisson's ratio and its associated dissipation. This parameter has often been assumed to be frequency independent (i.e., real valued). But since the elastic moduli are complex valued, Poisson's ratio also must be complex valued (Pimienta et al., 2016a). Poisson's ratio and its associated dissipation, measured for two effective pressures of 1 MPa and 10 MPa, are reported as a function of apparent frequency (Figure 5). Large frequency-dependent variations are observed on both properties at lowest effective pressure.

Poisson's ratio (Figure 5a) increases at low frequency then decreases beyond a frequency of about 10 Hz, leading to a bell-shaped variation. Again, the amount of dispersion highlighted by Poisson's ratio fully correlates with the large dissipation peaks measured (Figure 5b). The magnitude of dissipation measured is clearly larger than the one observed on K and E (Figure 4), implying that this property is in reality the one most affected by the frequency effects. Moreover, two clear dissipation peaks are observed at frequencies of 5 Hz and 500 Hz, i.e., very near although slightly below the values f_1^* = 10 Hz and f_2^* = 1 kHz (Figures 3 and 4). Thus, these values are consistent with fluid-flow theories.

How this bell-shaped variation measured for Poisson's ratio can be interpreted remains to be examined. If the maximum of the bell-shaped variation corresponds to the undrained regime, the undrained ν_{ud} would then be larger than the unrelaxed ν_{ur}. Effective-medium theories can be used to predict, in a simple way, the theoretical value of Poisson's ratio for the three elastic regimes in porous and microcracked rocks (e.g., Le Ravalec and Guéguen, 1996), assuming an isotropic medium. For this Fontainebleau sandstone sample, it can be shown that an effective pressure exists below in which the undrained Poisson's ratio is larger than the unrelaxed one (Pimienta et al., 2016a). A bell-shaped variation of Poisson's ratio is predicted to hold in rocks bearing a large density of microcracks, which is typically the case of sandstones.

Note finally that one property of main interest for the geophysics community, the V_P/V_S ratio, can be inferred directly from the

measured Poisson's ratio. Interestingly, the V_P/V_S ratio also exhibits a large bell-shaped variation in the frequency range of study (Pimienta et al., 2016a).

Artifacts due to the measurement system

Effect of the dead volume and measuring setup. For the stress-strain method, two approaches have been used to measure strains in rocks: the "global" LVDT measuring setup and the "local" strain-gauge measuring setup. Moreover, as shown by Dunn (1986), not using lateral bounding on a rock sample leads to measuring a lateral fluid flow out of the sample. Most existing apparatuses today use lateral bounding. In general, the sample is also bounded axially so that it can be considered undrained even at low frequencies. However, experimentally attaining a zero dead volume while simultaneously ascertaining a full sample saturation is difficult. A small dead volume would exist, for example, in the two end platens. But then, can the rock sample be assumed consistently to be undrained?

To investigate the artifacts due to the measurement system, a 1D poroelastic model has been developed by solving the differential equation satisfied by the pore pressure (Pimienta et al., 2016b). Three sets of boundary conditions have been tested: the theoretically drained and undrained boundary conditions, and the more realistic "experimentally undrained" boundary condition. This last boundary condition means that a dead volume exists at both sample ends, and the system "sample + dead volume" is undrained. Moreover, integrating either over the sample length (i.e., LVDT measurement) or over the strain-gauge length (i.e., strain-gauge measurement), insights on the comparison between "global" and "local" measurements can be obtained. From such modeling approach, (1) a strong dependence to the measuring setup (i.e., "global" LDVT versus "local" strain gauges) as well as to the measuring position is expected for the dispersion/attenuation measured; and (2) an interplay between sample and dead volume storage capacity will imply for the properties measured at lowest frequencies under liquid saturation to be in between purely drained and purely undrained.

The data for a Berea sandstone sample of 19% porosity (Pimienta et al., 2016b) have been checked against the 1D model (Figure 6). For the experiment, the dead volume is V_d = 6.6 mL, and the properties are measured locally with strain gauges. In conformity, the model predictions apply to the same experimental conditions. In addition, Figure 6 reports predictions (1) for a very large dead volume (i.e., drained boundary conditions); and (2) for the "global" responses. For this example, a good fit is obtained between model and measurement. Interestingly, for this sandstone sample, it is shown that the existence of a dead volume strongly affects the K value measured at low frequency. As a consequence, the measured dispersion/attenuation is strongly damped as compared to what would have been measured with drained boundary conditions. This dead-volume effect is expected to originate from the ratio between sample and dead-volume storage capacity. Note that "local" measurements (e.g., strain gauges) show a sharp frequency-dependent variation. Yet, "global" measurements (e.g., LVDT) are expected to show variations spread over four orders of frequency. Consistently, the magnitudes of the attenuation peaks are strongly damped.

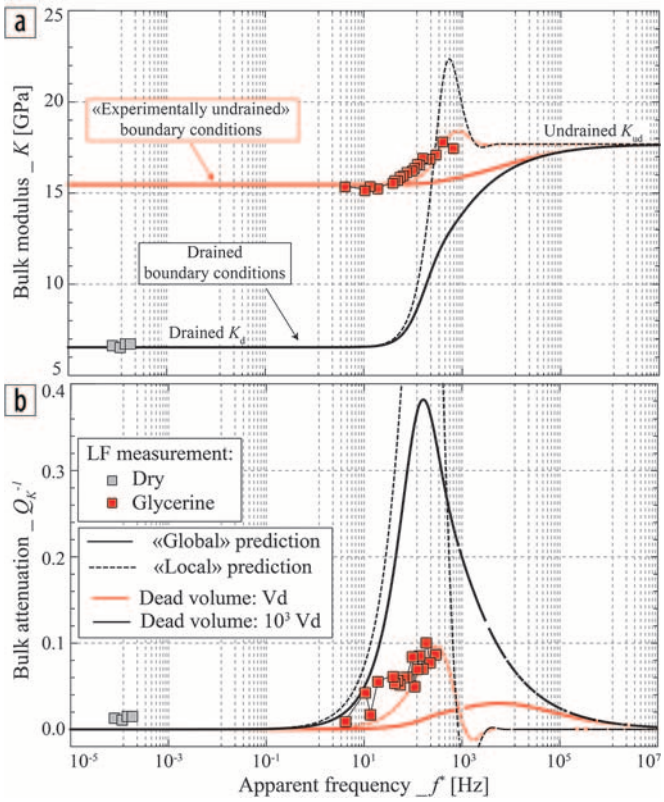

Figure 6. Comparison between the 1D poroelastic model predictions and the measurements on a Berea sandstone either dry or glycerine-saturated. The reported measurements are obtained with glued strain gauges at the sample center, and a dead volume of V_d = 6.6 mL. Accordingly, the "experimentally undrained" boundary condition is used with the value V_d, and properties are predicted "locally" at the sample canter. For comparison, the role of the "global" measurement (i.e., continuous curves) and drained (i.e., black curves) boundary conditions (i.e., dead volume >> V_d) are predicted. Figure modified from Pimienta et al. (2016b).

Note finally that the above model only applies to the drained/undrained transition. The question remains open for the undrained/unrelaxed transition.

Comparison between elastic properties measured. A last aspect to investigate is the comparison between the different elastic properties measured. It has been shown (Figures 4 and 5) that bulk modulus, Young's modulus, and Poisson's ratio showed dispersion/attenuation phenomena for two characteristic frequencies near the theoretically predicted f_1^* and f_2^*, i.e., for the drained/undrained and undrained/unrelaxed transitions, respectively. While the frequency dependence fits for all properties, it remains to verify if the magnitude of variations fits. The variations measured for the sample bulk modulus have been shown to perfectly fit Biot-Gassmann theory (Figure 3). Assuming that the shear modulus also fits with Biot-Gassmann theory and that the rock remains isotropic, it is possible to predict E and ν from K and G. For those predictions, we once again use the Zener rheologic model in order to predict E and ν as a function of apparent frequency. The predicted and directly measured Young's modulus and Poisson's ratio then are compared for two different effective pressures of 1 and 10 MPa (Figure 7).

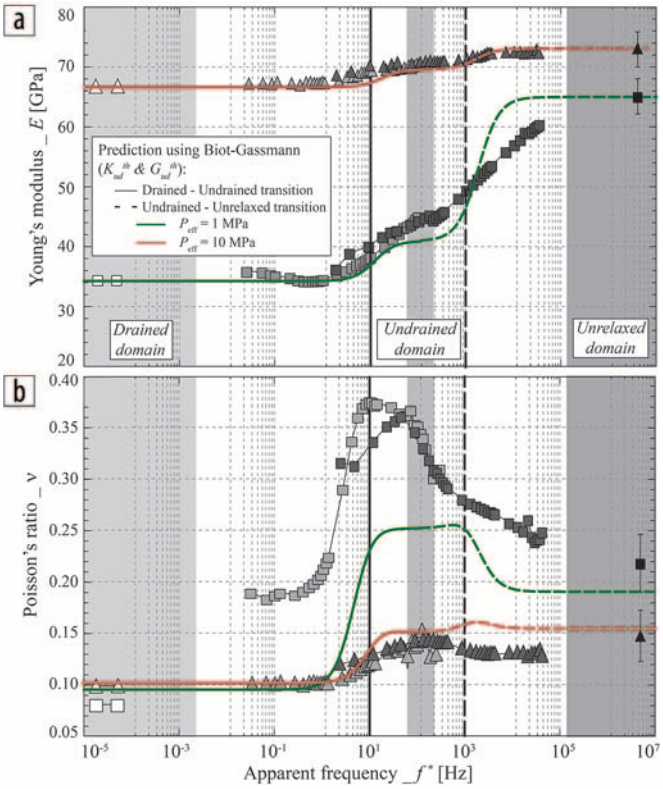

Figure 7. Comparison between predicted and directly measured (a) Young's modulus and (b) Poisson's ratio for the 7% porosity Fontainebleau sandstone sample at two effective pressures of 1 MPa and 10 MPa. The prediction is made using the values measured for the drained and unrelaxed regimes, and the ones fitting Biot-Gassmann theory for the undrained regime. The frequency dependence is obtained by using Zener rheologic model. Figure modified from Pimienta et al. (2015b; 2016a).

Both predicted Young's modulus and Poisson's ratio values appear to underestimate the values measured at P_{eff} = 1 MPa. The explanation for this difference remains to be explored. Note, however, that the fit is good at effective pressures above 5 MPa, i.e., as the rock microcracks close. A possible explanation would thus be a stress-induced anisotropy. Indeed, measurements of E and ν require an axial (i.e., anisotropic) stress oscillation that could modify the crack distribution.

If we assume a transverse isotropic (TI) symmetry, then two Young's moduli and Poisson's ratios exist. If the medium is anisotropic, we measure E_1 and ν_{12}. The properties inferred from isotropic conditions can be assumed to be near E_2 and ν_{21}. Thus, the experimental results show both relations of $E_1 > E_2$ (Figure 7a) and $\nu_{12} > \nu_{21}$ (Figure 7b). This is consistent with a TI medium's symmetry condition of $(E_1/\nu_{12}) = (E_2/\nu_{21})$.

Conclusion

Following the pioneering work of M. Batzle, different loss mechanisms can be found to cause dispersion/attenuation of elastic waves in fluid-saturated rocks. This work specifically investigates fluid-flow phenomena at different scales in fully saturated sandstones.

Two strong dispersions and attenuations phenomena have been measured on the bulk modulus, Young's modulus, and Poisson's ratio of a fully saturated Fontainebleau sandstone sample. Both in terms of characteristic frequency and of magnitude of the effects, the measurements are consistent with the usual fluid-flow and effective-medium theories. Direct measurement of both the cause (i.e., fluid flow out of the sample) and the consequence (i.e., dispersion and attenuation) of the transition between drained and undrained regimes are reported. Moreover, a second dispersion/attenuation phenomenon is also observed at higher frequencies, where no global fluid flow occurs. This second phenomenon is fully consistent with the undrained/unrelaxed transition.

Large frequency-dependent variations are measured on both bulk modulus and Young's modulus. Combining the measured moduli, it could be directly inferred that these transitions between regimes lead to a bell-shaped dispersion curve for Poisson's ratio. This is precisely what is observed from Poisson's ratio measurements. It is directly inferred that the V_P/V_S ratio is expected to also show large bell-shaped variations. An explanation for this variation is found from the use of effective-medium theories: for some rocks the undrained Poisson ratio is larger than the unrelaxed one. Again, the existing theories fit with the measurements both in terms of magnitudes of variations and characteristic frequencies for the variations. TLE

Acknowledgments

The authors wish to thank Y. Pinquier and A. Schubnel for their technical help in setting up the system. The authors also thank L. Adam and R. Hofmann for their constructive comments. Total has partially supported this work, under project no. FR00007429.

Corresponding author: pimienta@geologie.ens.fr

References

Batzle, M., R. Hofmann, D.-H. Han, and J. Castagna, 2001, Fluid and frequency dependent seismic velocity of rocks: The Leading Edge, **20**, no. 2, 168–171, http://dx.doi.org/10.1190/1.1438900.

Batzle, M., R. Hofmann, M. Prasad, G. Kumar, L. Duranti, and D.-H. Han, 2005, Seismic attenuation: observations and mechanisms: 75th Annual International Meeting, SEG, Expanded Abstracts, 1565–1568, http://dx.doi.org/10.1190/1.2147991.

Batzle, M., D.-H. Han, and R. Hofmann, 2006, Fluid mobility and frequency-dependent seismic velocity direct measurements: Geophysics, **71**, no. 1, N1–N9, http://dx.doi.org/10.1190/1.2159053.

Batzle, M., G. Kumar, R. Hofmann, L. Duranti, and L. Adam, 2014, Seismic-frequency loss mechanisms: Direct observations: The Leading Edge, **33**, no. 6, 656–662, http://dx.doi.org/10.1190/tle33060656.1.

Cleary, M. P., 1978, Elastic and dynamic response regimes of fluid-impregnated solids with diverse microstructures: International Journal of Solids and Structures, **14**, no. 10, 795–819, http://dx.doi.org/10.1016/0020-7683(78)90072-0.

Dunn, K.-J., 1986, Acoustic attenuation in fluid-saturated porous cylinders at low frequencies: The Journal of the Acoustical Society of America, **79**, 1709–1721, http://dx.doi.org/10.1121/1.393232.

Hofmann, R., 2006, Frequency dependent elastic and anelastic properties of clastic rocks: PhD thesis, Colorado School of Mines.

Le Ravalec, M., and Y. Guéguen, 1996, High-and low-frequency elastic moduli for a saturated porous/cracked rock — Differential

self-consistent and poroelastic theories: Geophysics, **61**, no. 4, 1080–1094, http://dx.doi.org/10.1190/1.1444029.
Müller, T. M., B. Gurevich, and M. Lebedev, 2010, Seismic wave attenuation and dispersion resulting from wave-induced flow in porous rocks: A review: Geophysics, **75**, no. 5, 75A147–75A164, http://dx.doi.org/10.1190/1.3463417.
O'Connell, R., and B. Budiansky, 1977, Viscoelastic properties of fluid-saturated cracked solids: Journal of Geophysical Research, **82**, no. 36, 5719–5735, http://dx.doi.org/10.1029/JB082i036p05719.
Pimienta, L., J. Fortin, and Y. Guéguen, 2015a, Bulk modulus dispersion and attenuation in sandstones: Geophysics, **80**, no. 2, D111–D127, http://dx.doi.org/10.1190/geo2014-0335.1.
Pimienta, L., J. Fortin, and Y. Guéguen, 2015b, Experimental study of Young's modulus dispersion and attenuation in fully saturated sandstones: Geophysics, **80**, no. 5, L57–L72, http://dx.doi.org/10.1190/geo2014-0532.1.
Pimienta, L., J. Fortin, and Y. Guéguen, 2016a, Effect of fluids and frequencies on Poisson's ratio of sandstone samples: Geophysics, **81**, no. 2, D35–D47, http://dx.doi.org/10.1190/GEO-2015-0310.1.
Pimienta, L., J. V. M. Borgomano, J. Fortin, and Y. Guéguen, 2016b, Role of the boundary conditions on the drained/undrained transition: Modelling the experiment, Geophysical Prospecting, **64**, no. 4, http://dx.doi.org/10.1111/1365-2478.12390.
Spencer Jr., J. W., 1981, Stress relaxations at low frequencies in fluid-saturated rocks: Attenuation and modulus dispersion: Journal of Geophysical Research, **86**, no. B3, 1803–1812, http://dx.doi.org/10.1029/JB086iB03p01803.